High power supercap electrodes based on vertical aligned carbon nanotubes on aluminum

S. Dörfler [a,b], I. Felhösi [c], T. Marek [c], S. Thieme [a,b], H. Althues [a,*], L. Nyikos [c], S. Kaskel [a,b]

[a] Fraunhofer Institute for Material and Beam Technology (IWS) Dresden, Winterbergstraße 28, 01277 Dresden, Germany
[b] Department of Inorganic Chemistry Dresden, University of Technology, Bergstraße 66, 01069 Dresden, Germany
[c] Institute of Materials and Environmental Chemistry, Research Centre for Natural Sciences, Hungarian Academy of Sciences, 1025 Budapest, Pusztaszeri ut 59-67, Hungary

HIGHLIGHTS

► Direct growth of up to 80 μm high vertical aligned CNT film on Al foil by efficient techniques was developed.
► Resulting VA-CNT/Al system is suitable for high power supercap electrodes.
► Higher capacities and lower resistances compared to nickel substrates were obtained.
► Cycle stability (300,000 cycles) compared to VA-CNT/nickel supercap electrodes was increased.

GRAPHICAL ABSTRACT
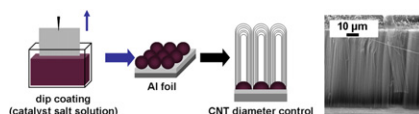
ARTICLE INFO

ABSTRACT

A scalable process at atmospheric pressure for direct growth of vertical aligned carbon nanotube (VA-CNT) on aluminum substrates has been developed including dip-coating steps for the wet-chemical buffer and catalyst layer deposition and a subsequent chemical vapor deposition step. Up to 80 μm high vertical aligned carbon nanotube forests were obtained on catalyst-coated aluminum foil in a thermal plasma-free CVD process at atmospheric pressure and 645 °C using ethene as carbon source. The influence of two catalyst compositions (Fe:Co 2:3 and Fe:Mo 47:3) and the effect of the catalyst concentration on growth rate, morphology and density of resulting CNT films were investigated. Additionally, the binder-free VA-CNT/ aluminum system was electrochemically tested as supercap electrode and the feasibility of tailoring the specific capacity varying the catalyst layer thicknesses was shown. The specific capacitance of electrodes deduced from impedance spectra varied between 25.6 and 61.2 F g^{-1} depending on the catalyst complex mixture composition and concentration. The VA-CNT/Al electrodes have a very low value of effective serial resistance (0.42–0.15 mΩ g) indicating a potential candidate as electrode material for high power supercapacitor application. Excellent cycle stability of supercapacitors has been demonstrated up to 300,000 cycles.

1. Introduction

The efficient synthesis of vertical aligned carbon nanotube (VA-CNT) films via CVD growth was discovered 2004 by Hata et al.

[1,2] and has been intensively studied since then. Most promising applications are field emission displays [3–5], lithium ion cells, optical polarizers [2,6], gas sensors [7], heat conductors, electrochemical double layer capacitors [2]. This latter was demonstrated in our earlier report [8] and we demonstrated VA-CNT/sulfur cathodes for Li/sulfur battery applications [9], as well. For the scalable production of such devices atmospheric pressure deposition techniques and direct synthesis on conductive substrates need to be developed. Due to the high thermal stability, nickel or steel

* Corresponding author. Tel.: +49 351 83391x3476; fax: +49 351 83391x3300.
E-mail addresses: susanne.doerfler@iws.fraunhofer.de (S. Dörfler), felhosi.ilona@ttk.mta.hu (I. Felhösi), marek.tamas@ttk.mta.hu (T. Marek), soeren.thieme@iws.fraunhofer.de (S. Thieme), holger.althues@iws.fraunhofer.de (H. Althues), nyikos.lajos@ttk.mta.hu (L. Nyikos), stefan.kaskel@chemie.tu-dresden.de (S. Kaskel).

substrates are the most favorite flexible metallic substrates for the CNT deposition [4,10,11]. For energy storage electrodes, aluminum is the most frequently used substrate due to its low mass density, high electrical conductivity and flexibility. Direct VA-CNT growth via thermal CVD on aluminum foil is limited by its melting point ranging between 640 and 660 °C depending on the respective alloy. While the deposition temperature can be reduced by using plasma enhanced CVD [12], this method does not seem to be very promising from an industrial point-of-view due to the high energy costs for the plasma generation. There are only few publications that reports direct growth of CNTs on aluminum (alloy) substrates. In these cases the success of preparation was limited regarding either the dense and uniform growth of high-quality VA-CNT arrays on aluminum, or the obtainable nanotube length, or the use of highly explosive carbon precursors like acetylene, or the reduced CVD process pressure that require more expensive equipments [13–18].

The aim of the present work was to grow vertically aligned carbon nanotubes with lengths of at least 50 μm on aluminum foil substrates without plasma treatment, by using carbon precursors at atmospheric pressure and within an appropriate deposition time. In short, the main question was that whether our preparation method [8] could be transferred from nickel foil to a more light-weight substrate materials, while retaining the control of the CNT morphology. This question rises inherently, as the melting point of Al require drastically lower temperatures than Ni. Naturally, the applicability of synthesized VA-CNT/Al samples as supercapacitor electrodes also should be tested. For the CVD growth of VA-CNT, substrates are typically covered by an Al_2O_3 buffer layer with the actual catalyst layer on top. Most frequently low-pressure physical vapor techniques are used for the deposition of Al_2O_3 buffer layers and Fe thin films as catalyst [1,19–22]. An alternative route is the wet-chemical catalyst deposition using metal nitrates, chlorides and acetates in polar organic solvents like ethanol and methanol [6,13,23–25] deposited mostly for low-pressure CVD processes or rather on polished silicon substrates. Precursor solutions can be applied via dip-coating which is essential for the development of scalable processes. In this work, binary thin layers of transition metal catalyst alloys (Fe/Co, Fe/Mo) were deposited on aluminum foils achieving CNT film heights up to 80 μm. We found that, according to our experience with Ni substrates, the CNT film thickness could be controlled by the growth time under these circumstances, as well. We also examined the need for an additional Al_2O_3 support layer − prepared from an Al precursor − in contrast to the native oxide layer. To establish the applicability of the as-prepared VA-CNT/Al samples as supercapacitor electrodes, we performed wide-scope electrochemical investigations, using a symmetric two-electrode test cell [8]. We found that in the case of Al substrates with Al_2O_3 support layers the specific capacity of the CNT material could be tailored by the catalyst film thickness using different Fe:Mo (47:3) salt concentrations in the 2-propanol dip-coating solution. As this finding is in good agreement with our previous results on nickel foils [8], the aim of the present work seems to be satisfied.

2. Experimental

The detailed deposition of the Al_2O_3 and oxidized Co, Fe and Mo alloy layers and the subsequent CVD process for the VA-CNT growth has already been described elsewhere [8,26]. Al_2O_3 layer thickness is 30 nm (estimated on polished silicon substrate by AFM) and values of the surface roughness are $R_a = 0.12$ and $R_q = 0.15$ (1×1 μm^2 scan size) so the surface morphology is very smooth.

For the deposition procedure on the metallic substrates aluminum foil (Alfa Aesar, 99.5% Al and Hydro, 99.99%) are cut into pieces of 4.5×4.5 cm^2 and primarily coated by a thin Al_2O_3 layer

and then by a film with the respective Fe/Co/Mo combination. To investigate the effect of the native Al_2O_3 layer only the transition metal layer was deposited as described previously. The substrates are cut into pieces of 3.5×3.5 cm^2 for the thermal CVD process, and 30 min growth time is applied for the investigation of the optimal catalyst composition and the experiments regarding the different temperatures. CNT lengths are controlled by variation of the growth time from 10 to 60 min at 645 °C controlled furnace temperature that corresponds to 635−645 °C substrate temperature. For 650 °C controlled furnace temperature, substrate temperatures between 640 and 650 °C are measured. In this work, the controlled furnace temperature is given.

The detailed characterization of the catalyst films by atomic force microscopy (AFM) and CNT films or rather scratched-off CNT (depending on the need of the method) by Raman spectroscopy, Scanning Electron Microscopy (SEM) and Transmission Electron Microscopy (TEM) are described in former publications. Furthermore, the equipment for measuring the specific surface area (SSA) has been reported elsewhere, as well [8,26]. The CNT film thickness or rather CNT heights was investigated by determining the height at five sample locations with a distance of approximately 5 mm. For each location, three different heights were determined and an average value was calculated. The CNT film thicknesses in the SEM images appear shorter due to 45° sample tilting. CNT (mass) density is estimated by weighting the substrates before and after the CVD process. Volume was calculated by CNT film height (SEM images) and the coated substrate size.

Electrochemical measurements were performed in a two-electrode flat cell. Details of the cell assembly have been described elsewhere [8]. Briefly, the symmetric electrochemical cell is composed of two identical CNT-coated Al foil electrodes (area of each electrode: 1×1 cm), with 25 μm-thick ethylcellulose separator between them, and 1 g tetraethylammonium tetrafluoroborate (TEABF$_4$)/10 ml acetonitrile as electrolyte.

Electrochemical measurements were performed with a Solartron 1286 electrochemical interface and a 1250 frequency response analyzer. The *impedance spectra* were obtained in the frequency range from 65 kHz to 100 mHz with 10 points per decade at different bias voltages using 10 mV amplitude. The data analysis was performed using Zwiev software by NLLS fitting impedance spectra to equivalent circuit models. The leakage resistance was determined from impedance spectra recorded in larger frequency range down to 10 mHz at 0 V and 2 V bias voltages. *Galvanostatic* charge/discharge measurements were done with different currents varying between 0.1 and 1 A g^{-1} relative to the mass of CNT in the active layer, with a voltage limitation between 0 and 2 V. The charging and discharging capacitance were determined by integration of corresponding voltage−time curves, while the cycle efficiency was determined by the ratio of discharge and charge capacitance. *Cyclic voltammograms* were measured in the potential window from −2 to 2 V at different scan rates of 10, 20, 50 and 100 mV s^{-1}. The cell capacitance values obtained in the symmetric cell configuration were recalculated also to a single electrode capacitance (i.e. which value can be measured in 3-electrode configuration). This latter is four times larger than the value of cell capacitance measured in a two-electrode cell configuration [8,27].

3. Results and discussion

As described in a previous publication, the applied process chain includes the wet-chemical buffer (Al_2O_3) or rather catalyst (oxidized Fe, Co and Mo) coating procedure and the subsequent CVD process [26] at 645 °C or 650 °C by using ethene as carbon precursor.
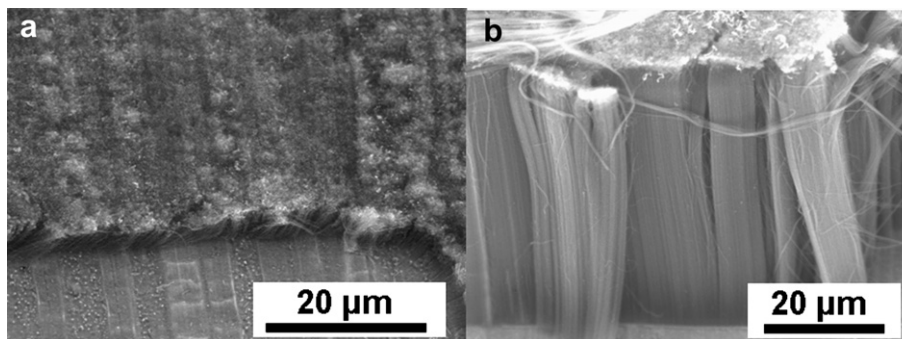
Fig. 1. SEM images of CNT generated by Fe:Co (2:3) catalyst with native aluminum foil (a) and with additional Al_2O_3 layer (b).

3.1. CNT films

Catalytic active transition metal (Fe, Co, Mo) [28] complex mixtures are subsequently deposited on the Al_2O_3 coated substrates and tested as catalyst in the CVD process at 645 °C. Homogeneous black coatings on the metal substrates are observed after at least 10 min CVD process. We optimized the catalyst compositions on nickel foil at 730 °C and observed the highest CNT films for the Fe:Co (2:3) binary catalyst system being discussed in detail elsewhere [26]. Additionally, a slight addition of Mo to pure Fe (6 mol%) led to the densest CNT forest due to a reduced Ostwald ripening behavior. Therefore, the latter catalyst system is also suitable for decreasing the catalyst concentration in the dip coating solution from 0.220 to 0.022 mol l^{-1} to control the CNT diameter indirectly [8].

Aluminum foil has a native Al_2O_3 layer being crucial for vertical aligned CNT growth [26], but the first experiments regarding VA-CNT synthesis on aluminum foil with native Al_2O_3 and Fe:Co (2:3) catalyst layer did not result in dense VA-CNT films. Only a thin film of more randomly oriented CNT could be generated (Fig. 1a).

In contrast, applying an additional Al_2O_3 layer underneath the Fe:Co (2:3) catalyst coating led to dense VA-CNT films with a height of 49 ± 11 µm after 30 min growth time Fig. 1b. The reason for this observation is given by AFM images: the untreated aluminum foil shows a remarkable higher surface roughness in nanometer scale than the additionally Al_2O_3 coated foil. The surface roughness value of a 5×5 µm scaled sample location (Supporting information S1) was calculated by the AFM Software as high as 52 nm for the untreated and 24 nm for the Al_2O_3 coated aluminum. The values of the surface roughness for 1×1 µm scan size (S2) are falsified by the micrometer-scaled roughness but the nano-scaled differences regarding the surface morphology are better observable using a scan size of 1×1 µm^2. The as-deposited catalyst layer agglomerates preferentially in the nanometer-scaled cavities of the untreated foil during heating up to 645 °C CVD temperature leading to an inhomogeneous CNT seed dispersion on the substrate. As consequence, CNT growth is more randomly orientated.

The optimized Fe:Co (2:3) system has been chosen to investigate the growth kinetics due to the highest growth efficiency. Fig. 2 shows the CNT film thickness control via different CVD process durations. Generally, CNT films on aluminum foil are thinner compared to those grown on nickel substrate due to the reduced temperature and the consequently decreased catalyst activity [29]. At 650 °C controlled furnace temperature, even high purity aluminum foil (99.99%) starts to melt at some sample locations.

10 min growth time lead to a CNT height of 14 µm (1.4 µm min^{-1}), 20 min to 25 ± 17 µm (1.25 µm min^{-1}); 30 min to 49 µm (1.7 µm min^{-1}) and 40 min to 81 µm (2 µm min^{-1}). Carbon nanotube growth becomes less efficient (1.0 µm min^{-1}) after

50 min for several reasons that have been already discussed for the deposition on nickel foil [26].

For 10 min deposition time, a CNT mass density of 0.27 ± 0.04 g cm^{-3} can be observed. For 20 min growth time, a slightly higher CNT density value of 0.31 ± 0.08 g cm^{-3} is calculated. For 30 min and 40 min growth time, CNT densities decrease to 0.15 ± 0.03 g cm^{-3} and 0.12 ± 0.02 g cm^{-3}, respectively. These findings are in accordance with the morphology changes during VA-CNT growth reported by Bedewy et al. [30]: In the initial stage randomly oriented CNT are primarily grown followed by a crowding process when CNT begin to grow vertically aligned. After this step, CNT density decreases to a certain point, when the CNT achieve the height maximum of 81 µm.

Interestingly, the quantity of "worm-like" filament structures on top of the CNT layer (Fig. 3) rises after process durations of 30 min and longer leading to higher density values of $0.16 \pm$ g cm^{-3} for 50 min and $0.20 \pm$ g cm^{-3} for 60 min, respectively.

The Specific Surface Area (SSA) of CNT generated by Fe:Co (2:3) system after 30 min is as high as 365 m^2 g^{-1} — slightly higher compared to CNT prepared by the same catalyst system on nickel foil and 20 min growth time (248 m^2 g^{-1}). Reason for this observation could be the reduced temperature and with it, the reduced particle Ostwald ripening to small CNT diameters and with it, a slightly higher SSA. Furthermore, no Ni atoms acting as catalyst metal are able to diffuse through the Al_2O_3 buffer layer and increase the catalyst particles.

VA-CNT grown by different deposition times was investigated by Raman spectroscopy: The ratio of the graphitic peak (G peak, 1580 cm^{-1}) and the peak representing disordered carbon (D peak, 1330–1360 cm^{-1}) strongly depends on the applied excitation laser wavelength λ_{laser}. Generally, the G/D peak area ratios measured by $\lambda_{laser} = 514$ nm are higher compared to 785 nm (Table 1 Supporting
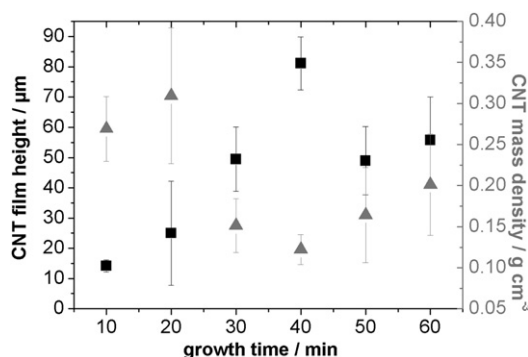

Fig. 2. Growth kinetics of CNT films on aluminum foil: CNT film thickness and mass density (including standard deviation) vs. growth time.
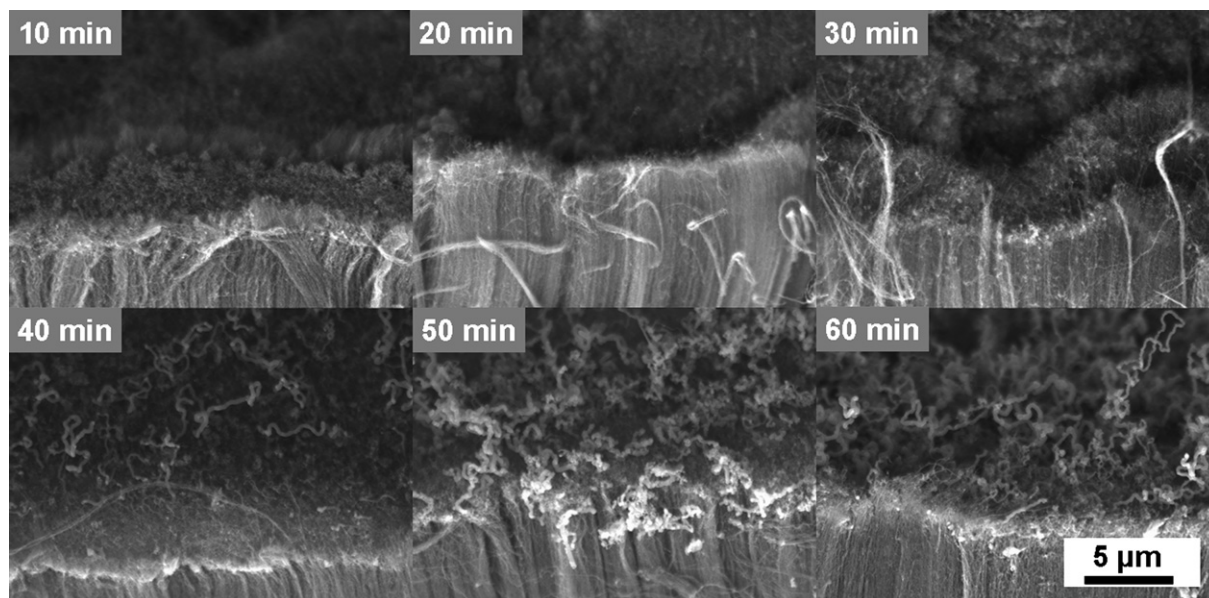
Fig. 3. SEM images of CNT tops with different growth times at 645 °C temperature generated by Fe:Co (2:3) catalyst system.

information), probably due to better resonance conditions [31]. Fig. 4 shows Raman spectra (λ_{laser} = 514 nm) and G/D peak area ratio of CNT generated by different growth times (Fe:Co (2:3) catalyst): Shape of G and D peak changes only slightly with longer CVD deposition until 40 min growth times. In contrast, the G/D peak area ratio decreases remarkably for 50 and 60 min CVD growth time from 0.8 to 0.6 probably due to the deposition of the as-mentioned "worm-like" carbon structures and the CNT etching by the water vapor leading to a lower graphitization degree.

No so-called "radial breathing modes" (RBM, 75–300 cm^{-1}) representing the single and double walled nanotubes with diameters between 1 and 2 nm were observed by using neither wavelengths for any of the CNT prepared by Fe:Co (2:3) catalyst system.

As can be seen in Fig. 5, for Fe:Mo (47:3) catalyst system, CNT films are remarkable thinner compared to the Fe:Co (2:3) system. With decreasing catalyst concentration (Figs. 5a and 6), CNTs grow more sparsely (0.05 g cm^{-3}) due to the presumed agglomeration of the catalyst film in the foil cavities. Additionally, for the lowest catalyst concentration, VA-CNTs are longer (29 ± 2 µm). For higher concentrations, as can be observed in Fig. 5b and c, VA-CNTs are shorter and grow denser (Fig. 6): 0.08 g cm^{-3} using 0.110 mol l^{-1} and 0.16 g cm^{-3} using 0.220 mol l^{-1} which agrees with our previous

report [8]. The film thickness drops with increasing catalyst concentrations since neighboring seeds generate a higher CNT quantity limiting the gas diffusion of the carbon precursor.

As can be seen in Fig. 7, only CNT generated by 0.022 mol l^{-1} catalyst concentration (corresponding to 2.8 nm layer thickness) show very small "RBM" intensity which indicates the presence of CNT with diameters from 1 to 2 nm. For CNT generated by all Fe:Mo (47:3) concentrations, G/D peak area ratio is as high as 0.3. For Fe:Co (2:3) system, the value for the G/D ratio is 0.25 revealing a lower graphitization degree being in good agreement with the TEM results.

The SSA of CNT generated by different Fe:Mo (47:3) concentrations could not be measured since the quantity of the active material scratched-off was remarkably lower compared to the Fe:Co (2:3) system due to the smaller CNT film thickness.

Fig. 8 shows TEM images of CNT grown by different catalyst concentrations (0.022–0.220 mol l^{-1}) of the Fe:Mo (47:3) system and 0.22 mol l^{-1} Fe:Co (2:3) system on aluminum foil: With increasing Fe:Mo (47:3) catalyst concentration, the quantity of CNT with higher diameter increases: For 0.022 mol l^{-1} catalyst concentration, an average CNT diameter of 5.6 ± 1.5 nm and for 0.110 mol l^{-1}, 6.8 ± 3.5 nm could be calculated from 50 CNT. CNT diameters of 9.8 ± 9.3 nm could be measured for 0.22 mol l^{-1} catalyst concentration being in good agreement to the remarkably lower specific capacity values showed in the next chapter. However, TEM images should not be over-interpreted since they only represent a very small sample spot. In contrast, electrochemical capacity measurements represent 2 cm^2 electrode and hence, approximately 2.8–3.6 × 10^{11} CNT (estimated after [32] and [33]). TEM (see also S3) reveals a relatively high quantity of amorphous carbon for the Fe:Co (2:3) catalyst system compared to the same concentration of the Fe:Mo (47:3) system that needs further investigation.
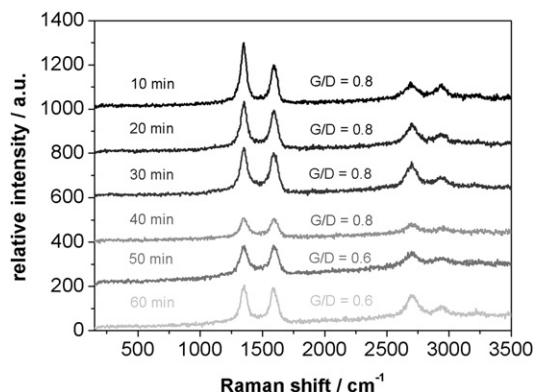
3.2. Electrochemical performance of supercapacitor cells composed of VA-CNT grown on aluminum substrate

The spectra were fitted with the equivalent circuit model consisting of an inductance of instrumentation (wires) L; a serial resistance representing the internal resistance of the capacitor R_S, determined by the electrolyte resistance with some contribution of
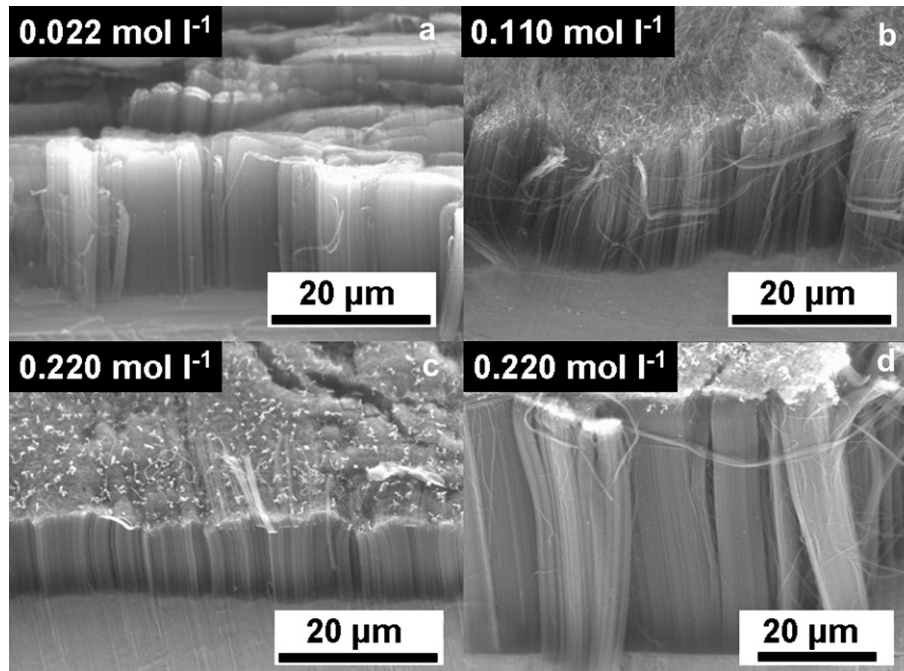

Fig. 4. Raman spectra and G/D peak area ratio of CNT generated by different growth times (Fe:Co (2:3) catalyst).

Fig. 5. Comparison CNT films (SEM) grown by three different catalyst concentrations of the optimized Fe:Mo (47:3) system (a–c) and 0.220 mol l^{-1} Fe:Co (2:3) system after 30 minutes growth time at 645 °C.

ohmic resistance of metal components and contact resistance between the active layer and substrate; and the impedance of the porous layer Z_{por}, known also as generalized finite Wartburg element, which can be expressed by the following equation [8,34]:

$$Z_{por}(\omega) = \left(\frac{R_W}{j\omega C}\right)^n \coth(j\omega R_W C)^n \qquad (1)$$

R_W represents the ion diffusion inside the pores, and C is the low frequency capacitance, corresponding to the double layer capacitance of the total pore surface area. The heterogeneity of the electrodes can be taken into consideration by the exponent of $n \leq 0.5$. At low frequencies Eq. (1) represents the serial connection of pore resistance ($R_{por} = R_W/3$) and a constant phase element (CPE) of double layer capacitance; while at high frequencies Eq. (1) gives the generalized Wartburg element. In an ideal case n is equal with 0.5, and Eq. (1) is identical with the de Levie impedance element [35], that represents a blocking porous electrode described by an RC-transition line model.

The impedance characteristics of VA-CNT electrodes are very close to ideal electrodes (see the typical impedance spectrum shown in Fig. 9a). At low frequencies, the electrode is dominated by pure capacitive characteristics; the exponent of CPE is very close to 1 ($2n = 0.96$) due to the homogenous aligned structure of CNT layer and the narrow distribution of pore diameter.

The knee frequency describes the value below a supercap electrode behaves capacitive. For CNT/Al supercap cells, this value is very high (approximately 1 kHz), which is beneficial for high frequency or high power application of supercapacitors. The knee-frequency of VA-CNT/Al exceeds even the values obtained for VA-CNT/Ni cells (50–200 Hz) [8]. If we calculate the apparent capacitance and resistance as a function of frequency (Fig. 9b), the optimal operation frequency range of supercapacitors built from VA-CNT/Al electrodes lies between 10 Hz–1 kHz. At $f < 10$ Hz, the apparent cell resistance increases due to the real part component of CPE and some contribution of parallel charge transfer resistance (leakage resistance). Consequently, the power density decreases at low frequencies. At $f > 1$ kHz, in the ion transport controlled regime, the capacitance decreases due to the lowered penetrability of pores inside the active layer, therefore the energy density drops, as well.
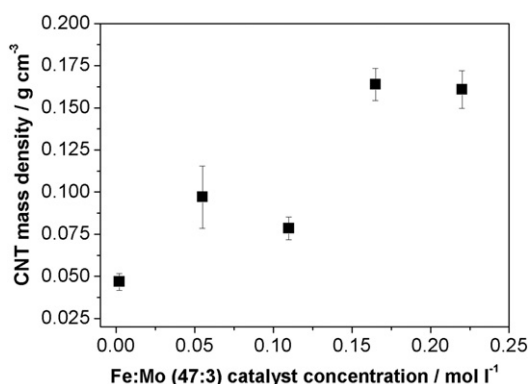
**Fig. 6.** CNT film mass density vs. concentration of the Fe:Mo (47:3) catalyst system.
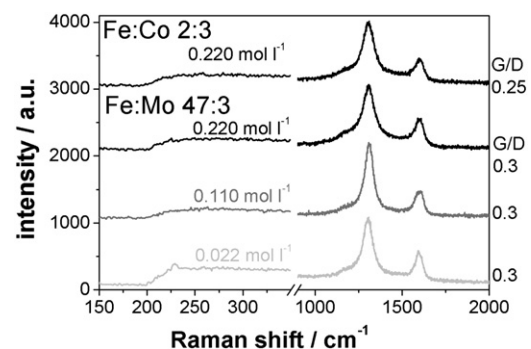
Fig. 7. Raman spectra of CNT grown by 0.22 mol l^{-1} Fe:Co (2:3) catalyst system and three different concentrations of Fe:Mo (47:3) catalyst system (0.022, 0.011 and 0.220 mol l^{-1}).
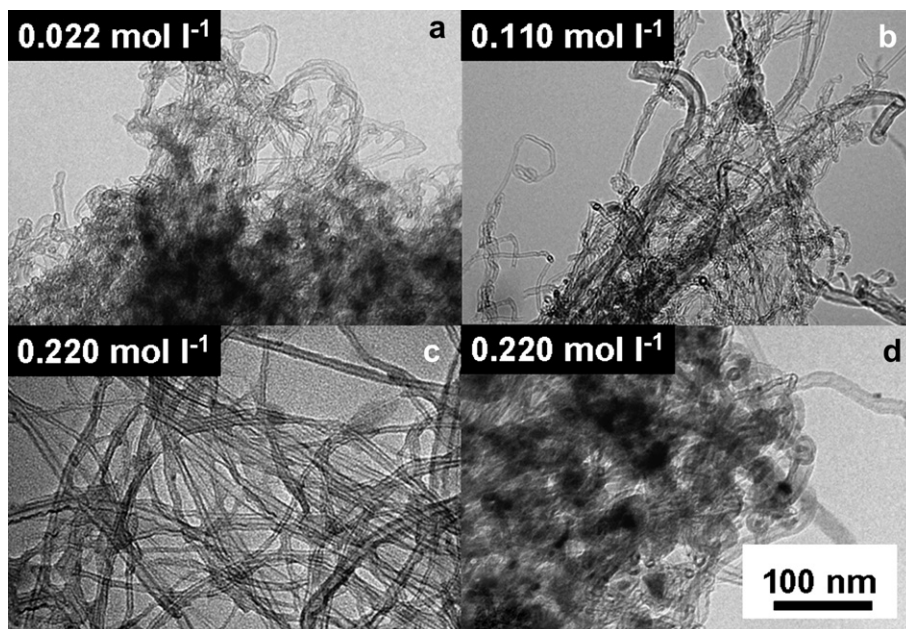
Fig. 8. TEM images of CNT grown by different catalyst concentrations (0.022–0.22 mol l^{-1}) of the Fe:Mo (47:3) system (a–c) and 0.22 mol l^{-1} Fe:Co (2:3) system (d) after 30 minutes growth time at 645 °C.

The double layer capacitance of CNT electrodes depends on the applied voltage as can be seen both on the fitted impedance data measured at different bias voltages (Fig. 9c) and on the cyclic voltammograms (Fig. 9d). The increase of capacitance with increasing voltage is a general characteristic of carbon materials in organic electrolytes [36–40] being attributed to several reasons. Salitra et al. [36] ascribe this observation to the potential dependence of the ion penetration into nano-scaled pores. Widely accepted
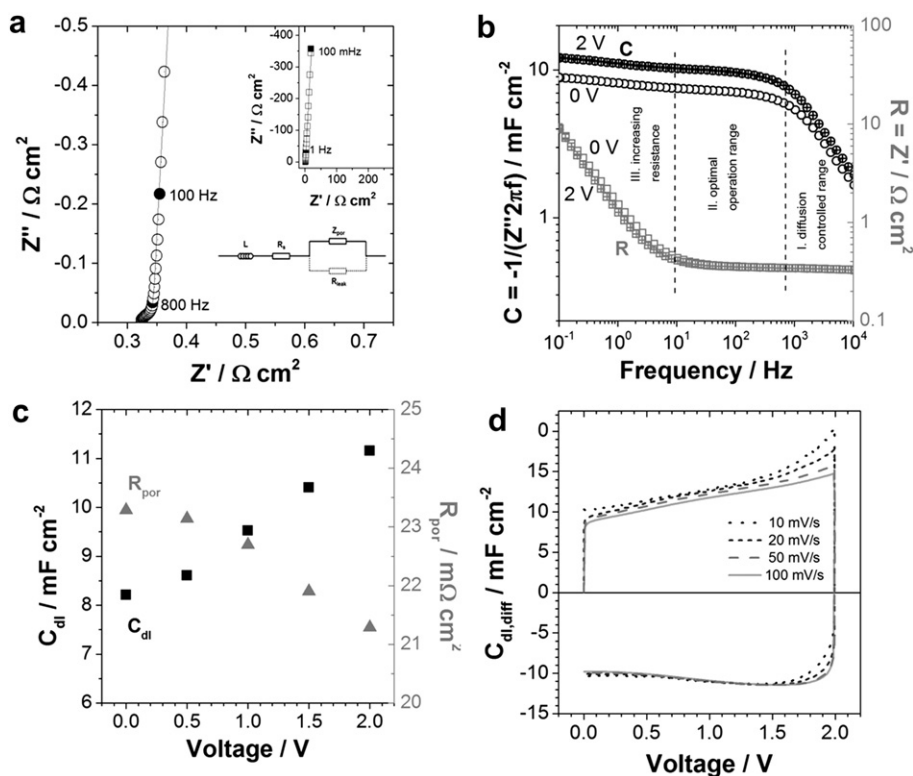
Fig. 9. (a) A representative complex plane impedance spectrum measured at 0 V bias in a two-electrode symmetrical cell made from aluminum substrate coated with CNT active layer, and inductance subtracted from the spectra. Solid lines are fitted spectra calculated by the equivalent circuit shown as inset. (b) Apparent normalized capacitance and resistance as a function of frequency; (c) the influence of applied voltage on the double layer capacitance and pore resistance; and (d) cyclic voltammetry curves in capacitance representation i.e. by plotting $C_{dl,diff} = I/Av$, where I is the measured current, A is the surface area and v is the sweep rate. (Data are obtained in a two-electrode symmetrical cell made from electrodes of 0.324 mg cm^{-2} CNT active layer grown by catalyst layer formed in 0.165 mol l^{-1} concentration of Fe-–Mo complex mixture).

Table 1
Applied catalyst complex concentrations, resulting CNT surface density after CVD process, and impedance data obtained with supercapacitor cells made from different VA-CNT electrodes.

| Catalyst composition	Fe:Co (2:3)	Fe:Mo (47:3)	Fe:Mo (47:3)	Fe:Mo (47:3)	Fe:Mo (47:3)	Fe:Mo (47:3)
Catalyst concentration [mol l^{-1}]	0.22	0.22	0.165	0.11	0.055	0.022
Oxidized catalyst thickness [nm]	23.8		18.4	12.0	4.4	2.8
CNT surface density [mg cm^{-2}]	0.369	0.401	0.324	0.222	0.148	0.136
Fitted impedance parameters at 0 V						
R_{el} [Ω cm^2]	0.3−0.5					
R_{por} [mΩ cm^2]	35.9	21.6	23.3	19.2	26.0	29.8
T_W [s^{2n}]	5.48*10^{-4}	6.3*10^{-4}	4.68*10^{-4}	2.88*10^{-4}	3.62*10^{-4}	4.25*10^{-4}
n	0.481	0.486	0.483	0.475	0.485	0.478
f_{knee} [Hz]	990	790	1130	2150	1080	1350
C_{dl} [mF cm^{-2}]	7.2	9.8	8.2	7.0	5.6	6.2
Fitted impedance parameters at 2 V						
R_{el} [Ω cm^2]	0.3 − 0.5					
R_{por} [mΩ cm^2]	28.4	24.4	21.3	16.8	24.9	28.2
T_W [s^{2n}]	7.44*10^{-4}	8.1*10^{-4}	5.8*10^{-4}	3.47*10^{-4}	4.5*10^{-4}	5.6*10^{-4}
n	0.479	0.486	0.482	0.475	0.484	0.479
f_{knee} [Hz]	740	610	920	1770	1150	1000
C_{dl} [mF cm^{-2}]	9.5	12.9	11.2	9.4	7.4	8.4
R_{ct} [kΩ cm^2]	1.31	33.1	18.7	16.3	12.4	8.5
Specific values calculated from impedance data at 2 V						
C_{sp} [F g^{-1}]	25.6	32.1	34.3	42.0	50.0	61.2
C_{cell} [F g^{-1}]	6.4	8.03	8.58	10.5	12.5	15.3
R_{esr} [mΩ g]	0.417	0.433	0.352	0.237	0.162	0.152
E [Wh kg^{-1}] (CNT mass)	3.56	4.08	4.77	5.83	6.94	8.50
P [kW kg^{-1}] (CNT mass)	2400	2310	2840	4220	6170	6580
E [Wh kg^{-1}] (cell mass)	0.114	0.142	0.135	0.114	0.091	0.102
P [kW kg^{-1}] (cell mass)	76.9	80.3	80.4	82.5	80.9	79.5

$CPE_{dl} = T_W/R_W$; $R_{por} = R_W/3$; $f_{knee} \approx 2.53/2\pi\ T_W^{1/(2n)}$; R_{esr} values are valid between 10 Hz−1 kHz.

explanation is the extension of the applied voltage into the carbon electrode causing a space charge [37–40], or the dielectric constant increases with voltage [40]. The electrolyte resistance is independent of the applied voltage, while the pore resistance slightly decreases at higher voltages (Fig. 9c). The latter can be explained by to the influence of the electric field on migration process of ionic species.

Table 1 summarizes the impedance results of VA-CNT/Al electrodes prepared by different catalyst compositions and concentrations. The catalyst composition and concentration has a significant influence on the CNT density and the double layer capacitance of electrodes. The VA-CNT/Al electrode obtained with Fe:Co (2:3) catalyst complex mixture have slightly lower double layer capacitance (9.5 mF cm^{-2} at 2 V) and higher pore resistance (28.4 mΩ cm^2 at 2 V) compared to the VA-CNT/Al electrode obtained by Fe:Mo (47:3) catalyst complex mixture with same 0.22 mol l^{-1} concentration (12.9 mF cm^{-2} and 24.4 mΩ cm^2, respectively). This is most probably due to the large amount of amorphous carbon present inside the nanotube layer as can be revealed by TEM images of Fig. 8. Consequently, electrochemical measurements prove the better applicability of Fe:Mo (47:3) catalyst mixture for the CNT growth on aluminum substrate.

The electrochemical measurements clearly show the feasibility of tailoring the specific capacitance of VA-CNT electrodes produced by scalable production techniques. As we discussed already in the previous chapter, the concentration of the optimized Fe:Mo (47:3) complex mixture influences the thickness of catalyst layer (see also Ref. [8]) and the CNT density grown by CVD. A quite good, almost linear relationship exists between the concentration and the resulted CNT surface density (Table 1). The normalized double layer capacitance per area increases with the concentration of catalyst solution (Fig. 10) and hence, with the density of CNT film, the highest value is obtained for 0.22 mol l^{-1} FeMo (12.9 mF cm^2) and the lowest value for 0.055 mol l^{-1} (7.4 mF cm^2), although the difference is lower than it would be expected from the difference between the CNT surface density (0.4 mg cm^2 and 0.15 mg cm^2,

respectively). The specific capacitance, at the same time, increases with decreasing concentration, and varies between 32.1 F g^{-1} (0.22 mol l^{-1}) and 61.2 F g^{-1} (0.022 mol l^{-1}), which suggests that a low catalyst film thickness (smaller particle size) formation of thinner CNTs can be realized by decreasing catalyst salt concentration. At low catalyst concentration (0.022 mol l^{-1}), the grown
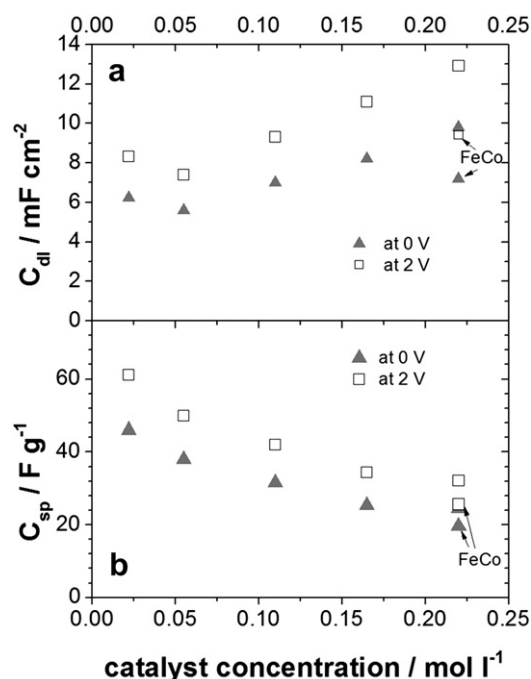
Fig. 10. The influence of catalyst concentration of Fe:Mo (47:3) complex mixture on (a) the normalized double layer capacitance and (b) specific capacitance of the VA-CNT layer grown on aluminium aluminum substrate. Data for Fe:Co (2:3) catalyst complex mixture is also inserted.

CNT forest layer exhibits a specific capacitance as high as 61.2 F g^{-1}; the corresponding cell capacitance is 15.3 F g^{-1}, which is $^3/_4$ part of the theoretically achievable value of SWCNT (20 F g^{-1}) in organic electrolytes [38,41,42]. As a consequence, small catalyst salt concentrations result in small catalyst particles which lead to a higher quantity of SWCNTs. At the same time, the surface density of the CNT layer is rather low, which is a drawback from an application-centered point of view as supercapacitor since the capacitance per area value is low. By increasing the catalyst concentration and producing higher amounts of MWCNTs, the specific capacitance decreases slightly but this is overcompensated by the increased density.

The specific capacitance values obtained on VA-CNT/Al electrodes are 1.6–2.6 times higher than the values obtained on VA-CNT/Ni electrodes [8] prepared with same catalyst concentrations of Fe:Mo (47:3) catalyst composition.

Several publications reported uniquely high specific capacitance for CNT. The specific capacitance of non-activated SWCNT may be as high as 80 F g^{-1} non-aqueous electrolytes such as Refs. [38,41,42]. Lin et al. investigated the capacitive energy storage of VA-CNT grown directly on aluminum foils via plasma-enhanced chemical vapor deposition [43] in ionic liquid electrolytes. They obtained high double layer capacitance as high as 8 mF m^{-2} in wide temperature range. Several papers reported high power thin layers of graphene and activated graphene [44,45] applicable at high frequency operation.

In contrast to the high gravimetric capacitance, the volumetric capacitance, or even more the double layer capacitance relating to the geometric surface area tends to be rather low, due to the loose packing of tubes [42]. This is detrimental in practical application, as larger electrode surface area is necessary to roll or fold obtaining the targeted nominal capacitance of supercapacitor device. Furthermore, the rate of several parasitic Faraday processes occurring in parallel is also dominantly determined by the geometric surface area of electrodes (such as decomposition of electrolyte, corrosion of current collector or metal substrate…). Therefore, beside the gravimetric capacitance, the double layer capacitance relating to the geometric surface area has to be taken into consideration during optimization of electrode materials for overall electrochemical performance of supercapacitor. Consequently, CNT electrodes with lower specific surface area but with denser packing of tubes may provide better overall electrochemical performance then the loose-packed SWCNTs.

The pore resistance of VA-CNT layers prepared on aluminum with different concentrations of Fe:Mo (47:3) catalyst mixtures is very low ($R_{por} \sim 20–30$ mΩ cm^2). This is a consequence of the high intrinsic conductivity of the nanotubes and ionic conductance in the interspaces of the VA-CNT. As a result, supercapacitors built from these electrodes are expected to provide a high specific power. Leakage resistance, which is the parallel charge transfer resistance of accompanying Faraday processes ranges between 8 and 33 kΩ cm^2 at 2 V bias voltage, and increases with the applied catalyst concentration. That means that the electrochemical performance of electrodes covered with denser CNT films is less influenced by accompanying electrochemical processes. We suppose that electrochemical processes dominantly take place on the bare aluminum surface resulting from gaps in the CNT layer. For lower catalyst concentrations, VA-CNT form more bundle-like structures due to the presumed agglomeration of the catalyst film in the cavities of the metal foil and the van der Waals forces between the tubes [46].

The integrated capacitance of CNT electrodes was also determined by from galvanostatic discharge curves measured by different currents (Fig. 11a). The specific capacitance decreases with increasing discharge current, which is the result of limited ion accessibility at high current operation. This tendency is valid for all investigated VA-CNT/Al electrodes. The galvanostatic cycle efficiency is also influenced by the charge–discharge current (Fig. 11b). The maximal cycle efficiencies of electrodes ranges between 0.92 and 0.96, and are reached with currents between 0.2 and 0.5 A g^{-1} (respective to the total CNT mass of the cell). The maximum-type shape of efficiency vs. current reflects a general electrochemical nature of electrodes: at lower currents the efficiency decreases due to the larger internal resistance of supercapacitor cell. In the other words: at lower currents, the charging time of capacitors is longer, and therefore the ratio of total charge participating in a parallel electrochemical reactions (such as decomposition of electrolyte, corrosion of current collector or metal substrate) − or dissipating due to heterogeneity − is higher, and hence, the energy loss is larger. This relationship is analogous to the increasing real part component of impedance with decreasing frequency marked as the III. frequency range in Fig. 9b. Above the optimal current ($I > 0.2–0.5$ A g^{-1}), the charging efficiency slightly drops with rising current: less fraction of the total pore surface area is charged at higher currents, while the internal resistance is nearly constant. The galvanostatic cycle efficiency is principally influenced by the mass of CNT per electrode area. The electrodes covered with denser CNT layer have significantly higher cycling efficiency. Reason for this is the increased capacitance per area, while the resistance normalized to the surface area is more-or-less independent of the CNT density.
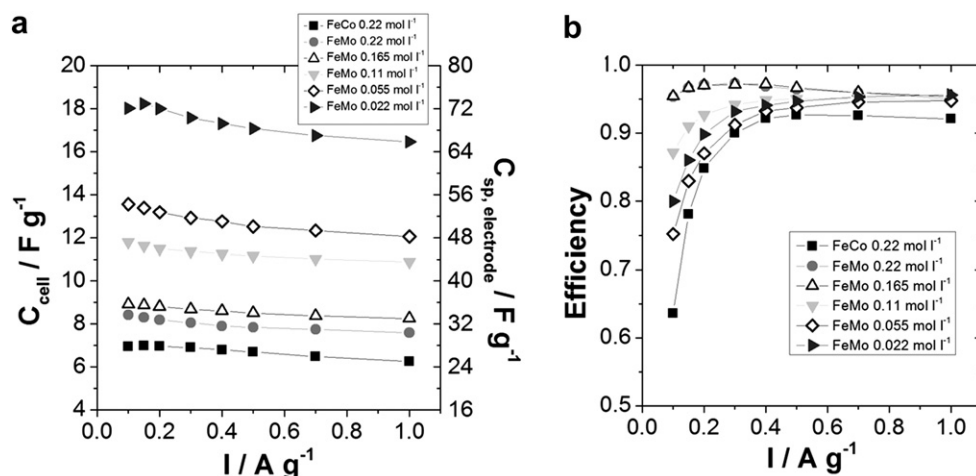

Fig. 11. (a) Discharge capacitance and (b) discharge/charge efficiency as a function of current obtained with cells of different VA-CNT/Al electrodes.

Another aspect is that the homogeneity of the denser CNT layer is also better (see the representative n values in Table 1).

Fig. 12a illustrates the long-term cycle stability of a super-capacitor cell built from $2 \times 1\ cm^2$ VA-CNT/Al electrodes being prepared with 0.165 mol l^{-1} FeMo catalyst mixture. The super-capacitor in this case is assembled as a hermetically sealed CR-2032 type coin cell. During the first 10,000 cycles, stabilization of supercapacitor cell occurs with slow logarithmic decrease of capacitance. The cell capacitance can be considered to be stable after 10,000 cycles, only very little −0.02%/1000 cycles decrease of capacitance observed up to 300,000 cycles. The cycle efficiency is also stable; its value is near constant at 0.935. The cyclic voltam-metry curves (Fig. 12b), measured after different GCD cycles as a fingerprint, prove that there is no significant change in the quality of the electrode properties. The minor decrease of capacitance is in accordance with the GCD results. The fitted impedance data reflects better the stability of supercap test device: the n value of the modified de Levie element (Fig. 12c), which describes the homo-geneity of the system, is constant, suggesting that there is no sign of degradation of electrode material at all. After an initial decrease, the parallel charge transfer resistance (leakage resistance) at 2 V is also constant, it levels around 50 kΩ cm^2 (Fig. 12d). The R_{ct} at 0 V is practically infinite. This suggests long-term cycle stability of the described CNT samples.

In summary, scalable wet-chemical deposition of an optimized Fe:Mo (47:3) complex mixture with different concentration proved to be suitable for controlling both the resulting CNT diameter and density of CNT films. As high as 61.2 F g^{-1} specific capacitance (deduced from the impedance spectra) was obtained with 0.022 mol l^{-1} complex mixture concentration. In contrast to the high specific capacitance, the capacitance per area of CNTs tends to be rather low due to the loose packing of tubes. This is detrimental

in practical application, as larger surface electrode area is necessary to obtain the targeted nominal capacitance of supercapacitor. Furthermore, the rate of several parasitic Faraday processes occurring in parallel is also dominantly determined by the geometric surface area of electrodes. Therefore, besides the gravi-metric capacitance, the normalized capacitance values have also to be taken into consideration in regard of electrode material opti-mization. Accordingly, denser CNT films − even if the ratio of MWCNTs is larger and the specific surface area is lower − result in better overall electrochemical performance for supercapacitor application.

The obtained electrochemical data allow us to estimate the two most important practical parameters of the supercapacitor cells − the energy density E and power density P. We gave two estima-tions of these parameters in Table 1, one for the mass of CNT-forest, and the more realistic one, which takes into account the cells' other components including the mass of CNT, mass of 50 μm thick aluminum substrate (thinner aluminum foils become very brittle during CVD treatment and are not suitable as substrate), the mass of separator and electrolyte, but excluding the cell house. The power density of the here described VA-CNT/Al EDLCs are approximately 80 kW kg^{-1}, and practically independent on the density of CNT layer. This is 1−2 magnitudes higher than the typical power density of supercapacitors made from activated carbon (AC) (0.5−10 kW kg^{-1}) [37]. This is due to the very low internal resis-tance of CNT EDLC owing to the fast ion-transfer process in the inter-tube channels of aligned CNT layers, high electronic conduc-tivity of the CNTs, and direct binder-free contact between CNT layer and aluminum substrate. On the other hand, the energy density varies between 0.1 and 0.15 Wh kg^{-1} depending on the density of the CNT layer. This is a magnitude lower than the energy density which can be reached with AC electrodes 1−10 Wh kg^{-1} [37]. The
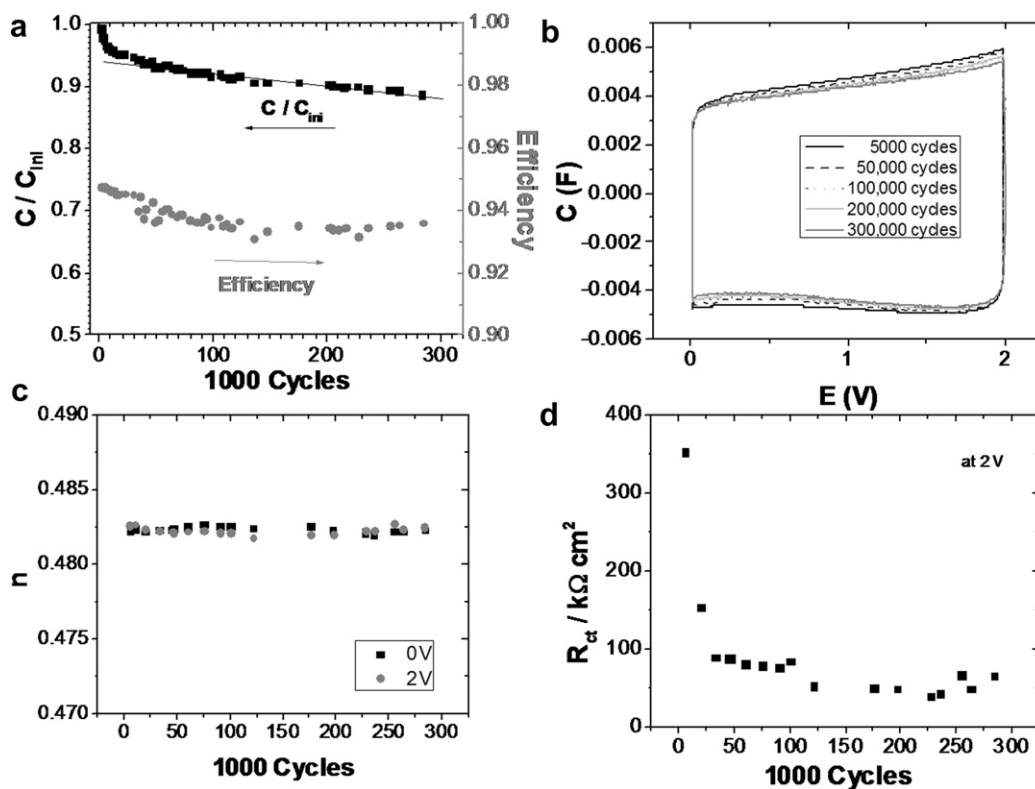
Fig. 12. (a) Galvanostatic charge/discharge cycle stability measured at constant current of 1 A g^{-1} for VA-CNT electrodes prepared with 0.165 mol l^{-1} Fe:Mo (47:3) complex mixture; (b) cyclic voltammetry curves in capacitance representation, (c) n element of modified de Levie parameter, and (d) parallel charge transfer resistance measured after given gal-vanostatic charge/discharge cycles.

Table 2
Comparison of results obtained for VA-CNT films on nickel and aluminum foil.

Parameter	VA-CNT/nickel	VA-CNT/aluminum
Furnace temperature	730 °C	645–650 °C
VA-CNT heights Fe:Mo (47:3) catalyst	100 μm	25 μm
VA-CNT heights Fe:Co (2:3) catalyst	170 μm	80 μm
CNT density Fe:Mo (47:3) catalyst	0.13 g cm^{-3}	0.16 g cm^{-3}
CNT density Fe:Co (2:3) catalyst	0.07 g cm^{-3}	0.15 g cm^{-3}
CNT diameter or Fe:Mo (47:3)	4.5 ± 1.1 nm for 0.022 mol l^{-1}	5.6 ± 1.5 nm 0.022 mol l^{-1}
	20.5 ± 5.8 nm for 0.22 mol l^{-1}	9.8 ± 9.3 nm for 0.22 mol l^{-1}
Capacity obtained from impedance (2 V)	37 F g^{-1} for 0.022 mol l^{-1}	61 F g^{-1} for 0.022 mol l^{-1}
	12 F g^{-1} for 0.22 mol l^{-1}	32 F g^{-1} for 0.22 mol l^{-1}
Pore resistance	30–58 mΩ cm^2	17–28 mΩ cm^2
Knee frequency	50–200 Hz	740–1000 Hz
Cycle stability of capacitance (galvanostatic charge/discharge	Up to 50,000 cycles	>300,000 cycles

major reason of the lower energy density is the loose packing of tubes in the active layer resulting low density 0.15–0.4 mg cm^{-2}, in contrary to the AC based electrodes having a typical active mass loading around 10 mg cm^{-2}. Our electrochemical results indicate the advantage of VA-CNT supercapacitors in applications that require high power density or high frequency.

4. Conclusion

In conclusion, the transfer of efficient wet-chemical deposition techniques of two optimized (co) catalyst systems from nickel as a kind of model support to aluminum substrates was successful. Table 2 summarizes all important values for both nickel and aluminum foil as current collector and reveals that especially density, capacity and resistance values were remarkably improved for supercap applications.

A simple thermal CVD process for the growth of CNT forests on aluminum substrate at atmospheric pressure, without plasma treatment and without highly explosive carbon precursors (such as acetylene) resulting in very high CNT films (80 μm) was developed. CNT growth could be optimized regarding growth time, catalyst composition and concentration in the dip coating solution. The chemical solution deposition allows thereby alloying catalysts just by mixing the required metal complex solutions to control the CNT morphology and to tailor the catalyst layer thickness and with it the resulting CNT diameters. The precursors are affordable and available and the dip-coating process as well as the APCVD process has the potential for up-scaling in a continuous process. Electrochemical measurements clearly show the feasibility of tailoring the specific capacity of vertical aligned CNT films being produced by scalable production techniques. The specific capacitance deduced from impedance spectra varied between 25.6 and 61.2 F g^{-1} depending on the catalyst complex mixture composition and concentration. To our knowledge, the combination of facile process techniques, very high CNT films directly grown on aluminum foil with up to 80 μm high CNT and the possibility of tailoring CNT diameters on a rough support is unique and has not been published elsewhere.

The VA-CNT electrodes have a very small value of effective serial resistance at 0.42–0.15 mΩ g and exhibited good cycling stability (up to 300,000 cycles). These results indicate that the as-synthesized VA-CNT layers on aluminum foil could be a potential candidate as electrode material in high power supercapacitors and reveal improved properties compared to VA-CNT on nickel foil.

Appendix A. Supporting information

Supplementary data related to this article can be found at http://dx.doi.org/10.1016/j.jpowsour.2012.11.068.

References

[1] K. Hata, D.N. Futaba, K. Mizuno, T. Namai, M. Yumura, S. Iijima, Science 306 (2004) 1362.
[2] K. Hata, S. Iijima, M. Yumura, D. Futaba, US Patent 2008/0318049 A1.
[3] T. Yamada, T. Namai, K. Hata, D.N. Futaba, K. Mizuno, J. Fan, M. Yudasaka, M. Yumura, S. Iijima, Nature Nanotechnology 1 (2006) 131.
[4] T. Hiraoka, T. Yamada, D.N. Futaba, H. Kurachi, S. Uemura, M. Yumura, S. Iijima, Journal of the American Chemical Society 128 (2006) 13338.
[5] Y.M. Wong, W.P. Kang, J.L. Davidson, B.K. Choi, W. Hofmeister, J.H. Huang, Diamond and Related Materials 14 (2005) 2078.
[6] Y. Murakami, S. Chiashi, Y. Miyauchi, M. Hu, M. Ogura, T. Okubo, S. Maruyama, Chemical Physics Letters 385 (2004) 298.
[7] W.S. Cho, S.-I. Moon, K.-K. Paek, Y.-H. Lee, Sensors and Actuators B 119 (2006) 180.
[8] S. Dörfler, I. Felhősi, I. Kék, T. Marek, H. Althues, S. Kaskel, L. Nyikos, Journal of Power Sources 208 (2012) 426.
[9] S. Dörfler, M. Hagen, H. Althues, J. Tübke, S. Kaskel, M.J. Hoffmann, Chemical Communications 48 (2012) 4097.
[10] R. Guzman de Villoria, A.J. Hart, B.L. Wardle, ACS Nano, http://dx.doi.org/10.1021/nn2008645 2011.
[11] C. Masarapu, B. Wie, Langmuir 23 (17) (2007) 9046.
[12] Z.Q. Tian, S.H. Lim, C.K. Poh, Z. Tang, Z. Xia, Z. Luo, P.K. Shen, D. Chua, Y.P. Feng, Z. Shen, J. Lin, Advanced Energy Materials 1 (2011) 1205.
[13] N. Yoshikawa, T. Asari, N. Kishi, S. Hayashi, T. Sugai, H. Shinohara, Nanotechnology 19 (2008) 245607.
[14] Ch Emmenegger, P. Mauron, A. Züttel, Ch Nützenadel, A. Schneuwly, R. Gallay, L. . Schlapach, Applied Surface Science 162 (2000) 452.
[15] R. Kavian, A. Vicenzo, M. Bestetti, Journal of Materials Science 46 (2011) 1487.
[16] C. Emmenegger, J. Bonard, P. Mauron, P. Sudan, A. Lepora, B. Grobety, Carbon 41 (2003) 539.
[17] Z.L. Gao, K. Zhang, M.M.F. Yuen, Nanotechnology 22 (2011) 265611 (8 pp).
[18] Z. Kai, M.M.F. Yuen, D.G.W. Xiao, Y.Y. Fu, P. Chan, Electronic Components and Technology Conference (2008) 1659.
[19] A.J. Hart, A.H. Slocum, Journal of Physical Chemistry B 110 (2006) 8250.
[20] S. Chakrabarti, H. Kume, L. Pan, T. Nagasaka, Y. Nakayama, Journal of Physical Chemistry C 111 (2007) 1929.
[21] S. Noda, K. Hasegawa, H. Sugime, K. Kakehi, Z. Zhang, S. Maruyama, Y. Yamaguchi, Japanese Journal of Applied Physics 46 (17) (2007) L399.
[22] Y. Yun, V. Shanov, Y. Tu, S. Subramaniam, M. Schulz, Journal of Physical Chemistry B 110 (2006) 23920.
[23] M. Someya, T. Fuji, US Patent 2003/0211029A1.
[24] M. Hu, Y. Murakami, M. Ogura, S. Maruyama, T. Okubo, Journal of Catalysis 225 (2004) 230.
[25] L. Zhang, Y. Tan, D.E. Resasco, Chemical Physics Letters 422 (2006) 198.
[26] S. Dörfler, A. Meier, S. Thieme, P. Németh, H. Althues, S. Kaskel, Chemical Physics Letters 511 (2011) 288.
[27] D. Qu, H. Shi, Journal of Power Sources 74 (1998) 99–107.
[28] S. Esconjauregui, C.M. Whelan, K. Maex, Carbon 47 (2009) 659.
[29] A. Moisala, A.G. Nasibulin, E.I. Kauppinen, Journal of Physics: Condensed Matter 15 (2003) S3011.
[30] M. Bedewy, E.R. Meshot, M.J. Reinker, A.J. Hart, ACS Nano 5 (11) (2011) 8974.

[31] H. Kataura, Y. Kumazawa, Y. Maniwa, I. Umezu, S. Suzuki, Y. Ohtzuka, Y. Achiba, Synthetic Metals 103 (1999) 2555.
[32] D.N. Futaba, K. Hata, T. Namai, T. Yamada, K. Mizuno, Y. Hayamizu, M. Yumura, S. Iijima, Journal of Physical Chemistry B 110 (2006) 8035.
[33] S.H. Kim, G.W. Mulholland, M.R. Zachariah, Carbon 47 (2009) 1297.
[34] R. Kötz, M. Carlen, Electrochimica Acta 46 (2000) 2483.
[35] R. De Levie, in: P. Delaray, C.T. Tobias (Eds.), Advances in Electrochemistry and Electrochemical Engineering, vol. 6, Interscience, NY, 1967, p. 329.
[36] G. Salitra, A. Soffer, L. Eliad, Y. Cohen, D. Aurbach, Journal of the Electrochemical Society 147 (2000) 2486.
[37] A.G. Pandolfio, A.F. Hollenkamp, Journal of Power Sources 157 (2006) 11.
[38] P.W. Ruch, L.J. Hardwick, M. Hahn, A. Foelske, R. Kötz, A. Wokaun, Carbon 47 (2009) 38.
[39] M. Hahn, M. Baertschi, O. Barbieri, J.-C. Sauter, R. Kötz, R. Gallay, Electrochemical and Solid-State Letters 7 (2004) A33.
[40] F. Rafik, H. Gualous, R. Gallay, A. Crausaz, A. Berthon, Journal of Power Sources 165 (2007) 928–934.
[41] D.N. Futaba, K. Hata, T. Yamada, T. Hiraoka, Y. Hayamizu, Y. Kakudate, O. Tanaike, H. Hatori, M. Yumura, S. Iijima, Nature Materials 5 (2006) 987.
[42] P.W. Rutz, R. Kötz, A. Wokaun, Electrochimica Acta 54 (2009) 4451–4458.
[43] R. Lin, P.L. Taberna, S. Fantini, V. Presser, C.R. Perez, F. Malbosc, N.L. Rupesinghe, K.B.K. Teo, Y. Gogotsi, P. Simon, Journal of Physical Chemistry Letters 2 (2011) 2396–2401.
[44] J.R. Miller, R.A. Outlaw, B.C. Holloway, Science 329 (2010) 1637–1639.
[45] Y. Zhu, S. Murali, M.D. Stoller, K.J. Ganesh, W. Cai, P.J. Ferreira, A. Pirkle, R.M. Wallance, K.A. Cychosz, M. Thommes, D. Su, E.A. Stach, R.S. Ruoff, Science 332 (2011) 1537–1541.
[46] P. Nikolaev, M.J. Bronikowski, R.K. Bradley, F. Rohmund, D.T. Colbert, K.A. Smith, R.E. Smalley, Chemical Physics Letters 313 (1999) 91.